PHYSICAL REVIEW D VOLUME 12, NUMBER 9 1 NOVEMBER 1975

Inclusive cross sections and angular distributions in Reggeon field theory*

Henry D. I. Abarbanel and Jochen Bartels
Fermi National Accelerator Laboratory,† Batavia, Illinois 60510

J. B. Bronzan and D. Sidhu
Department of Physics, Rutgers University, New Brunswick, New Jersey 08903
(Received 23 June 1975)

We use the Reggeon field-theory rules for inculsive reactions to study those processes in the triple-Regge region. We first show that at asymptotic energies the dominant Reggeon graphs have a single Pomeron connected to external fast particles. We construct the sum of these dominant graphs by obtaining the infrared forms of the Pomeron propagator and triple-Pomeron vertex. This is done by an expanded set of renormalization-group equations which allow one to determine the separate dependencies on all momenta and energies. As a by-product we obtain the momentum-transfer dependence of $d\sigma/dt$ in $2\to2$ processes. The inclusive cross section is discussed in detail as to its dependence on momentum transfer and missing mass, and we verify that there is no violation of s-channel unitarity when Pomerons interact among themselves. We also estimate the energy at which our asymptotic forms start to become valid.

I. INTRODUCTION

In a companion paper[1] we have given rules for calculating the effects of multi-Pomeron cuts on inclusive processes in the triple-Regge limit. Here we shall use those rules, together with the renormalization group, to calculate the inclusive cross section in the triple-Regge limit. As a by-product of the calculation we obtain the diffraction peak in $2\to2$ amplitudes.

In Ref. 1 we used the hybrid diagram technique of Gribov[2] to obtain the "Reggeon calculus" rules in the triple-Regge limit. As in the case of $2\to2$ processes,[3,4] it is t-channel unitarity which requires the cuts to be determined by these rules. (This point is made directly by Cardy, Sugar, and White,[5] who derive the "Reggeon calculus" in the triple-Regge limit using t-channel unitarity alone.) s-channel unitarity has not been used at all, so one must check to see whether it is or can be satisfied. One of the most sensitive checks is the requirement that the cross section for events in the triple-Regge region not exceed the total cross section. This requirement is not met by a simple Pomeron pole with $\alpha(0)=1$ and $\alpha'(0)$ finite.[6] What we require then is that the effects of the cuts restore s-channel unitarity in this restricted form. The cuts are strong, and we shall find that unitarity is indeed restored.

In Sec. II we use the renormalization group to prove that the dominant contribution to the inclusive cross section is due to Reggeon diagrams in which a single Pomeron is attached to the external fast particles. As a consequence, the inclusive cross section factorizes at sufficiently high energy. A similar result has been found for $2\to2$ amplitudes.[7] In both cases, the effect follows from the manner in which the product of a number of Pomeron field operators at a point is renormalized. As the number of Pomerons coming together increases, the dimension of the product changes, introducing a factor which suppresses diagrams with multiple emission of Pomerons by external particles.

In Sec. III we begin the study of the dominant contribution. Here we encounter a problem which is connected with the large number of independent variables for an inclusive cross section. If we copy the treatment of $2\to2$ amplitudes,[7] we obtain a scaling law, Eq. (29). However, a single scaling law becomes less and less interesting as the number of variables increases. For example, the scaling law for $2\to2$ amplitudes is enough to determine the energy dependence of $\sigma_{\text{total elastic}}$, but the scaling law for inclusive reactions in the triple-Regge region is insufficient to determine the contribution of such events to the total cross section. In Sec. III we therefore apply great effort to the calculation of the scaling function which appears in the scaling law. A simple technique for calculating scaling functions was introduced in Ref. 7, and we first show why it is not really satisfactory. The trouble with this technique is that it is not uniformly valid in the neighborhood of $J=1$ and $t=0$. We develop new formulas in Sec. III which overcome this defect. The presentation in Sec. III is for the Pomeron propagator, which is one element we need for the dominant contribution to the inclusive cross section. The calculation is lengthy, but it results in real improvements. We can now give detailed angular distributions in both $2\to2$ and inclusive cross sections. The scaling law seems to suggest that the propagator has a fixed cut at $J=1$, but our new formu-

las show that there are only the moving Regge-Mandelstam cuts. Our formulas also have some conceptual interest in that they show what can be learned from the renormalization group by studying the dependence of Green's functions on the most general normalization point.

In Sec. IV we complete the construction of the dominant contribution by calculating the energy-nonconserving triple-Pomeron vertex. Here again, the scaling function is obtained. In Secs. II to IV we calculate to lowest order in the ϵ expansion, where $\epsilon = 4 - D$, and $D = 2$ is the number of transverse dimensions in a high-energy collision. From experience with the scaling exponents, we expect the lowest term in the ϵ expansion to give the qualitative predictions of Reggeon field theory at $D = 2$, and we expect the quantitative predictions to be correct to within a factor of perhaps 3.[8,9]

In Sec. V we evaluate the inclusive cross section in the triple-Regge limit and exhibit our results in various forms. We also verify that the integrated inclusive cross section grows no more rapidly with energy than the total cross section.

Section VI is devoted to conclusions and a summary of what we have accomplished. We estimate the energies at which our asymptotic formulas should hold, and find they *probably* are not applicable at presently accessible energies. Nevertheless, the formulas we derive have considerable utility. We are able to check s-channel unitarity, as discussed above. The distributions we calculate have all the qualitative features seen in the data. For example, in $2 \to 2$ processes there is a shrinking exponential diffraction peak which dominates the second diffraction maximum by six orders of magnitude. Since we know cuts are strong, it is not obvious until the calculation is done that the interacting Pomeron will lead to a forward Regge pole-like distribution of this sort. Another noteworthy feature of our results is that the inclusive differential cross section is nonzero at $t = 0$. Therefore, if one insists on fitting inclusive data with a simple Pomeron pole in the triple-Regge region, we do not expect the phenomenological triple-Pomeron vertex to vanish. (We emphasize that the triple-Pomeron vertex *does* vanish at $t_i = 0$, $J_i = 1$. When cuts are present, the inclusive cross section does not vanish at $t = 0$ because $J_i \neq 1$ contributes to the Sommerfeld-Watson transform.) Our results agree with other treatments of the inclusive cross section in Reggeon field theory where they overlap.[10]

II. THE RENORMALIZATION GROUP AND THE INCLUSIVE AMPLITUDE IN THE TRIPLE-REGGE LIMIT

The inclusive cross section for the process $p_1 + p_2 \to p_1' + X$ is given by the formula

$$\frac{d\sigma}{dt\,dM^2} = \frac{1}{32i\pi s^2} \operatorname*{Disc}_{s_1 = M^2} T_6(s_{12} = s + i\epsilon, s_{13} = s - i\epsilon, s_1 = M^2, t_1 = 0, t_2 = t_3 = t). \tag{1}$$

The six-point amplitude T_6 has the kinematic identifications shown in Fig. 1. The triple-Regge limit is

$$\frac{s}{M^2} \to \infty, \quad \frac{M^2}{m_0^2} \to \infty, \quad t \text{ fixed}. \tag{2}$$

In this limit T_6 has several contributions, of which one has a discontinuity in s_1.[1] This contribution is given by the Sommerfeld-Watson integral

$$T_6(s_{12}, s_{13}, s_1, t_i) = \int_{c-i\infty}^{c+i\infty} \frac{dJ_1 dJ_2 dJ_3}{(-2i\pi)^3} \left(\frac{s_{12}}{m_0^2}\right)^{J_2} \left(\frac{s_{13}}{m_0^2}\right)^{J_3} \left(\frac{s_1}{m_0^2}\right)^{J_1 - J_2 - J_3} \xi_{J_2} \xi_{J_3} \xi_{J_1 - J_2 - J_3} F(J_1, J_2, J_3, t_i). \tag{3}$$

The signature factors are

$$\xi_{J_i} = \frac{e^{-i\pi J_i} + \tau_i}{\sin \pi J_i},$$

$$\xi_{J_1 - J_2 - J_3} = \frac{e^{-i\pi(J_1 - J_2 - J_3)} + \tau_1 \tau_2 \tau_3}{\sin \pi (J_1 - J_2 - J_3)}. \tag{4}$$

For Pomerons all signatures are positive, $\tau_i = 1$. The inclusive cross section is therefore

$$\frac{d\sigma}{dtdM^2} = \frac{1}{16\pi s^2} \int_{c-i\infty}^{c+i\infty} \frac{dJ_1 dJ_2 dJ_3}{(2i\pi)^3} \xi_{J_2} \xi_{J_3}^* \left(\frac{s}{M^2}\right)^{J_2+J_3} \left(\frac{M^2}{m_0^2}\right)^{J_1} F(J_1, J_2, J_3, t). \tag{5}$$

As in Ref. 1, we shall replace the angular momentum and momentum variables by energies $E = 1 - J$ and two-dimensional spacelike momenta $\vec{q}$, $\vec{q}^2 = -t$. We also replace $\xi_{J_2} \xi_{J_3}^*$ by $|\xi_1|^2 = 1$. In terms of these variables,

$$\frac{d\sigma}{dtd\ln M^2} = \frac{1}{16\pi} \int_{c-i\infty}^{c+i\infty} \frac{dE_1 dE_2 dE_3}{(2i\pi)^3} F(E_1, E_2, E_3, t_2 = t_3 = -\vec{q}^2) \exp\left[-E_1 \ln \frac{M^2}{m_0^2} - (E_2 + E_3) \ln \frac{s}{M^2}\right]. \tag{6}$$

The rules for calculating the partial-wave amplitude F are given in Ref. 1. They are stated as Reggeon perturbation rules:

(1) Draw all topologically distinct Pomeron digraphs (graphs with arrows on Pomeron propagators) in which energy E_1 enters and energies E_2 and E_3 exit. Only triple-Pomeron vertices are included, but any number of Pomerons may couple at a point to external particles. An example is shown in Fig. 2.

(2) For each diagram, identify the "notable" vertices. A notable vertex has one incoming and two outgoing lines. In addition, notable vertices have a topological property which can be stated in terms of paths following arrows and leaving the vertex. The property is that no path starting with one line leaving a notable vertex ever meets a path starting with the other line leaving the notable vertex. Notable vertices are identified on the Reggeon diagram in Fig. 2.

(3) At each vertex put $r_0/(2\pi)^{(D+1)/2}$.

(4) For a coupling to external particles in which s Pomerons come together put $(i)^{s-1} N_{0,s}/(2\pi)^{(D+1)(s-1)/2}$.

(5) For each Pomeron momentum $\vec{k}$ and energy E use the propagator

$$G_0^{(1,1)}(E, \vec{k}) = \frac{i}{E - \alpha_0' \vec{k}^2 + i\epsilon}. \tag{7}$$

(6) For each elementary two-Pomeron loop put a factor $\frac{1}{2}$.

(7) Choose one of the notable vertices at which energy will not be conserved. A diagram having k notable vertices makes k contributions in which energy nonconservation occurs at a different notable vertex. (For some diagrams, the contributions with different notable vertices chosen as energy nonconserving will be topologically identical. Even in this case, each contribution must be retained. See Sec. V of Ref. 1 for an example.)

(8) Conserve momentum at vertices and energy at non-notable vertices. Energy is not conserved at the energy-nonconserving vertex chosen in step (7). At other notable vertices insert a factor

$$\delta^+(E_{\text{in}} - E_{\text{out}}) = i/(2\pi)(E_{\text{in}} - E_{\text{out}} + i\epsilon). \tag{8}$$

(9) Integrate $d^D k\, dE$ over remaining internal momenta and energies.

(10) Multiply by $i\,(2\pi)^{(D+1)/2}$ for over-all normalization.

In these rules, D is the number of transverse dimensions. Physically, $D = 2$. No intercept renormalization is required to maintain $\alpha(0) = 1$ within the ϵ expansion.

We now want to study the infrared behavior of particular contributions I_{s_1,s_2,s_3} to the partial-wave amplitude F. I_{s_1,s_2,s_3} is the sum of all Reggeon diagrams with s_1 Pomerons connected to the par-

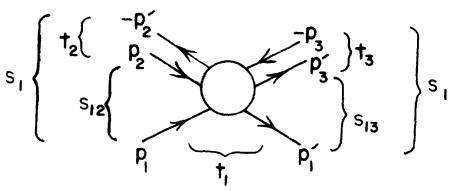

FIG. 1. Kinematics of the six-point amplitude which is related to the inclusive cross section. In the inclusive process $s_1 = M^2$ is the missing mass, $s_{12} = s_{13} = s$ is the total energy, $t_2 = t_3 = t$ is the momentum transfer, and $t_1 = 0$.

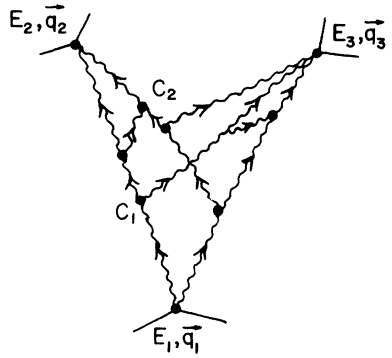

FIG. 2. A Reggeon diagram with two notable vertices at C_1 and C_2.

ticles where E_1 enters the diagram and s_2 (s_3) Pomerons connected to the particles where E_2 (E_3) leaves the diagram. In order to begin, we introduce the renormalized contribution I_{R,s_1,s_2,s_3}. This is calculated in the same way as I_{s_1,s_2,s_3}, but with the elements in perturbation theory replaced as follows:

Propagators: $\frac{i}{E-\alpha_0'\vec{k}^2+i\epsilon} \to \frac{iZ_3^{-1}}{E-Z_2\alpha_0'\vec{k}^2+i\epsilon}$,

Vertices: $r_0 \to Z_1 r_0$,

External couplings: $N_{0,s} \to Z_{s+3}N_{0,s}$.

It follows that

$$I_{R,s_1,s_2,s_3}(E_i, \vec{q}, r_0, \alpha_0', N_{0,s_1}, N_{0,s_2}, N_{0,s_3}) = I_{s_1,s_2,s_3}(E_i, \vec{q}, Z_1 Z_3^{-3/2} r_0, Z_2\alpha_0', Z_3^{-s_1/2}Z_{s_1+3}N_{0,s_1}, Z_3^{-s_2/2}Z_{s_2+3}N_{0,s_2}, Z_3^{-s_3/2}Z_{s_3+3}N_{0,s_3}). \quad (9)$$

We define renormalized couplings and slope by

$$r = Z_3^{3/2}Z_1^{-1}r_0,$$
$$N_s = Z_3^{s/2}Z_{s+3}^{-1}N_{0,s}, \quad (10)$$
$$\alpha' = Z_2^{-1}\alpha_0'.$$

Then we have

$$I_{R,s_1,s_2,s_3}(E_i, \vec{q}, r, \alpha', N_{s_1}, N_{s_2}, N_{s_3}) = I_{s_1,s_2,s_3}(E_i, \vec{q}, r_0, \alpha_0', N_{0,s_1}, N_{0,s_2}, N_{0,s_3}). \quad (11)$$

This gives the invariance of the contribution I under renormalization.

The renormalization constants are chosen by placing normalization conditions on the renormalized proper vertices introduced in Ref. 7. The proper vertices are one-Reggeon irreducible Green's functions for m incoming and n outgoing Reggeons, with external propagators amputated. Renormalized and unrenormalized vertices are related in a manner implied by perturbation theory rules,

$$\Gamma_R^{(n,m)}(E_i, \vec{q}_i, r, \alpha') = (Z_3)^{(n+m)/2}\Gamma^{(n,m)}(E_i, \vec{q}_i, r_0, \alpha_0'). \quad (12)$$

(We remind the reader that proper vertices contain only energy-conserving vertices.) Therefore, by placing appropriate normalization conditions on the renormalized vertices, we can fix the Z's. The conditions we choose are those of Ref. 7:

$$\left.\frac{\partial i\Gamma_R^{(1,1)}}{\partial E}\right|_{E=-E_N,\ \vec{k}^2=0} = 1, \quad (13a)$$

$$\left.\frac{\partial i\Gamma_R^{(1,1)}}{\partial \vec{k}^2}\right|_{E=-E_N,\ \vec{k}^2=0} = -\alpha', \quad (13b)$$

$$\Gamma_R^{(2,1)}|_{E_1=2E_2=2E_3=-E_N,\ \vec{k}_i=0} = r/(2\pi)^{(D+1)/2}. \quad (13c)$$

From these equations we learn that

$$Z_3^{-1} = \left.\frac{\partial i\Gamma^{(1,1)}}{\partial E}\right|_{E=-E_N,\ \vec{k}^2=0}, \quad (14a)$$

$$Z_2^{-1} = -(\alpha_0')^{-1}Z_3\left.\frac{\partial i\Gamma^{(1,1)}}{\partial \vec{k}^2}\right|_{E=-E_N,\ \vec{k}^2=0}, \quad (14b)$$

$$Z_1^{-1} = (2\pi)^{(D+1)/2}(r_0)^{-1}\Gamma^{(2,1)}|_{E_1=2E_2=2E_3=-E_N,\ \vec{k}_i=0}. \quad (14c)$$

We do not have to introduce a separate renormalization constant for energy-nonconserving triple-Regge vertices. If we did, the normalization condition would be like Eq. (14c), but $\Gamma^{(2,1)}$ would be replaced by $\tilde{\Gamma}^{(2,1)}$, where the tilde indicates the presence of one energy-nonconserving vertex in each perturbation diagram for $\tilde{\Gamma}^{(2,1)}$, and a δ^+ at other notable vertices in $\tilde{\Gamma}^{(2,1)}$. However, when external energy is conserved, as it is in Eq. (14c), $\tilde{\Gamma}^{(2,1)} = \Gamma^{(2,1)}$, and the new charge renormalization constant equals Z_1.[1]

The renormalization constants Z_{s+3} are fixed by placing normalization conditions on renormalized proper couplings to external particles. These are one-Reggeon irreducible amplitudes for two incoming particles and s outgoing Reggeons, with external Reggeon propagators amputated. In calculating Z_{s+3} we take $N_{0,s}$ to be the only nonzero bare coupling. Renormalized and unrenormalized coupling functions are related by

$$\Lambda_{R,s}(E_i, \vec{q}_i, r, \alpha', N_s) = (Z_3)^{s/2}\Lambda_s(E_i, \vec{q}_i, r_0, \alpha_0', N_{s,0}). \quad (15)$$

The normalization conditions and renormalization constant are

$$\Lambda_{R,s}|_{E_i=-E_N,\ \vec{q}_i=0} = N_s(i)^{s-1}/(2\pi)^{(D+1)(s-1)/2}, \quad (16)$$

$$Z_{s+3}^{-1} = (2\pi)^{(D+1)(s-1)/2}(N_{0,s})^{-1}\Lambda_s|_{E_i=-E_N,\ \vec{q}_i=0}(i)^{1-s}. \quad (17)$$

Since Λ depends linearly on $N_{0,s}$, Z_{s+3} has no dependence on this parameter.[11]

A renormalization-group equation can be derived for I_{R,s_1,s_2,s_3} by noting that the right side of Eq. (9) has no dependence on E_N. By applying the chain rule we find

$$\left[E_N\frac{\partial}{\partial E_N}+\beta\frac{\partial}{\partial g}+\zeta\frac{\partial}{\partial\alpha'}+(s_1+s_2+s_3)\frac{\gamma}{2}-\gamma_{s_1}-\gamma_{s_2}-\gamma_{s_3}\right]I_{R,s_1,s_2,s_3}=0. \tag{18}$$

In writing this we have replaced r by the dimensionless coupling constant

$$g=\frac{r}{(\alpha')^{D/4}}(E_N)^{D/4-1}. \tag{19}$$

The coefficients are

$$\begin{aligned}&\beta=E_N\frac{\partial g}{\partial E_N},\quad \zeta=E_N\frac{\partial\alpha'}{\partial E_N},\\ &\gamma=E_N\frac{\partial\ln Z_3}{\partial E_N},\quad \gamma_s=E_N\frac{\partial\ln Z_{s+3}}{\partial E_N}.\end{aligned} \tag{20}$$

In these derivatives, the bare parameters r_0 and α_0' are held fixed. We can use the dimensional arguments advanced in Ref. 7 to derive the representation

$$I_{R,s_1,s_2,s_3}=N_{s_1}N_{s_2}N_{s_3}(E_N)^{-2}\left(\frac{E_N}{\alpha'}\right)^{(D/4)(s_1+s_2+s_3-4)}\psi_{s_1,s_2,s_3}\left(\frac{E_i}{E_N},\frac{\alpha'\vec{q}^2}{E_N},g\right). \tag{21}$$

From this it follows that

$$\left(\xi\frac{\partial}{\partial\xi}+\alpha'\frac{\partial}{\partial\alpha'}+E_N\frac{\partial}{\partial E_N}+2\right)I_{R,s_1,s_2,s_3}(\xi E_i,\vec{q},g,\alpha',E_N)=0. \tag{22}$$

Combining this with Eq. (18), we obtain a scaling equation

$$\left[\xi\frac{\partial}{\partial\xi}-\beta\frac{\partial}{\partial g}+(\alpha'-\zeta)\frac{\partial}{\partial\alpha'}+2+\gamma_{s_1}+\gamma_{s_2}+\gamma_{s_3}-(s_1+s_2+s_3)\frac{\gamma}{2}\right]I_{R,s_1,s_2,s_3}(\xi E_i,\vec{q},g,\alpha',E_N)=0. \tag{23}$$

The solution of Eq. (23) is

$$\begin{aligned}I_{R,s_1,s_2,s_3}(\xi E_i,\vec{q},g,\alpha',E_N)&=I_{R,s_1,s_2,s_3}(E_i,\vec{q},\bar{g}(-\ln\xi),\bar{\alpha}'(-\ln\xi),E_N)\\ &\times\exp\int_{-\ln\xi}^{0}dt\left[\left(\frac{s_1+s_2+s_3}{2}\right)\gamma(\bar{g}(t))-\gamma_{s_1}(\bar{g}(t))-\gamma_{s_2}(\bar{g}(t))-\gamma_{s_3}(\bar{g}(t))-2\right],\end{aligned} \tag{24}$$

where $\bar{g}$ and $\bar{\alpha}'$ satisfy the ordinary differential equations

$$\begin{aligned}&\frac{d\bar{g}(t)}{dt}=-\beta(\bar{g}(t)),\quad \bar{g}(0)=g,\\ &\frac{d\bar{\alpha}'(t)}{dt}=\bar{\alpha}'(t)-\zeta(\bar{\alpha}'(t),g(t)),\quad \bar{\alpha}'(0)=\alpha'.\end{aligned} \tag{25}$$

In Reggeon field theory, this equation is useful when $\beta(g)$ has a zero with $d\beta/dg>0$. Let us suppose g_1 is such a zero. Following the standard analysis, we find a scaling law for the infrared behavior of I (see Ref. 7):

$$\begin{aligned}I_{R,s_1,s_2,s_3}&=(E_N)^{-2}\left(\frac{E_N}{\alpha'}\right)^{(D/4)(s_1+s_2+s_3-4)}\left(\frac{-E}{E_N}\right)^{Q}\\ &\times\phi_{s_1,s_2,s_3}\left[\frac{E_i}{E},\frac{\alpha'\vec{q}^2}{E_N}\left(\frac{-E}{E_N}\right)^{-z(g_1)}\right].\end{aligned} \tag{26}$$

Here E is a linear combination of the E_i, and

$$\begin{aligned}Q&=-2+Z(g_1)\frac{D}{4}(s_1+s_2+s_3-4)\\ &\quad+\tfrac{1}{2}\gamma(g_1)(s_1+s_2+s_3)\\ &\quad-\gamma_{s_1}(g_1)-\gamma_{s_2}(g_1)-\gamma_{s_3}(g_1),\\ Z(g_1)&=1-\frac{\zeta(\alpha',g_1)}{\alpha'}.\end{aligned} \tag{27}$$

Equation (26) can be restated

$$I_{R,s_1,s_2,s_3}(\lambda E_i, \lambda^{z(g_1)}\vec{q}^2) = \lambda^Q I_{R,s_1,s_2,s_3}(E_i, \vec{q}^2). \tag{28}$$

From Eqs. (6) and (28) we obtain a scaling law for the inclusive cross section which holds for large M^2/m_0^2 and s/M^2:

$$\frac{d\sigma}{dt\,d\ln M^2}\left(\lambda \ln\frac{s}{M^2}, \lambda \ln\frac{M^2}{m_0^2}, t\right) = \lambda^{-3-Q}\frac{d\sigma}{dt\,d\ln M^2}\left(\ln\frac{s}{M^2}, \frac{\ln M^2}{m_0^2}, \lambda^{z(g_1)}t\right). \tag{29}$$

This shows the shrinkage of the inclusive diffraction pattern, and that the contribution I with the lowest index Q dominates at high energy. Note that further work will be required to determine the shape of the diffraction pattern.

We will compute Q in the ϵ expansion. When $D=4$, $g_1=0$. For $\epsilon = 4-D$ small, there will still be a zero of β with g_1 small, and we will work to lowest order in ϵ. This means we calculate β to order ϵg and $\epsilon^0 g^3$, and the other renormalization-group functions to order $\epsilon^0 g^2$. Some of the functions have been calculated before,[7]

$$\beta = -\frac{\epsilon g}{4} + \frac{6g^3}{4(8\pi)^{D/2}},$$
$$\zeta = -\frac{\alpha' g^2}{4(8\pi)^{D/2}}, \tag{30}$$
$$\gamma = -\frac{g^2}{2(8\pi)^{D/2}}.$$

The anomalous dimensions associated with the couplings at a point to external particles are calculated to order $\epsilon^0 g^2$ using the $s(s-1)$ diagrams of Fig. 3. The expression is

$$\gamma_s = -\frac{s(s-1)g^2}{(8\pi)^{D/2}}. \tag{31}$$

We thus find, to order ϵ,

$$\frac{g_1^2}{(8\pi)^{D/2}} = \frac{\epsilon}{6}, \quad \gamma(g_1) = -\frac{\epsilon}{12}, \quad Z(g_1) = 1 + \frac{\epsilon}{24},$$
$$\gamma_s = -\frac{\epsilon}{6}s(s-1),$$
$$Q = -3 + \frac{\epsilon}{12} + \left(1 - \frac{\epsilon}{4}\right)(s_1+s_2+s_3-3) + \frac{\epsilon}{6}[s_1(s_1-1)+s_2(s_2-1)+s_3(s_3-1)]. \tag{32}$$

We see from this that the leading contribution at high energy comes from the contribution with $s_1=s_2=s_3=1$, which is illustrated in Fig. 4. The leading contribution factorizes, as it does in the four-particle amplitude and total cross section.[7]

In Ref. 7, the *four-particle* amplitude was analyzed in terms of Reggeon contributions $I_{n,m}$, in which n Reggeons are emitted by one pair of particles, and m Reggeons are collected by the other pair. The analysis of $I_{n,m}$ is analogous to what we have done here. However, in Ref. 7, γ_s was erroneously omitted. When it is included, one obtains for the asymptotic four-particle amplitude

$$\mathrm{Im}T(s,t) \sim s\left(\ln\frac{s}{m_0^2}\right)^{-\gamma(g_1)} \sum_{m,n=1}^{\infty} \tilde{F}_{m,n}\left[t\left(\ln\frac{s}{m_0^2}\right)^{z(g_1)}\right]\left(\ln\frac{s}{m_0^2}\right)^{-(n+m-2)[\gamma(g_1)/2+(D/4)z(g_1)]+\gamma_n(g_1)+\gamma_m(g_1)}. \tag{33}$$

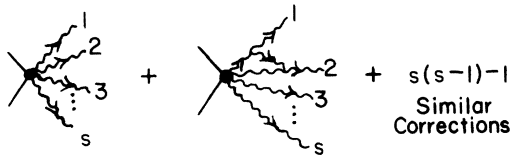

FIG. 3. Diagrams which must be evaluated to calculate the anomalous dimension of the coupling to external particles.

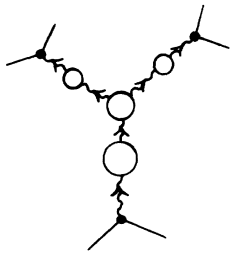

FIG. 4. The leading asymptotic contribution to the inclusive cross section.

This equation corrects Eq. (112) of Ref. 7. None of the conclusions of that paper is affected.

III. THE POMERON PROPAGATOR

One element in the dominant contribution is the complete Pomeron propagator. To calculate it we must determine the momentum and energy dependence explicitly. The techniques used in Sec. II and Ref. 7 must be altered to accomplish this. Let us begin by showing precisely how those techniques are inadequate.

In Ref. 7, by using the arguments of Sec. II, a scaling law was deduced for the infrared behavior of the renormalized inverse propagator

$$\Gamma_R^{(1,1)}(E,\vec{k},g_1,\alpha',E_N) = E_N\left(\frac{-E}{E_N}\right)^{1-\gamma(g_1)}\phi_{1,1}\left[\left(\frac{-E}{E_N}\right)^{-Z(g_1)}\frac{\alpha'\vec{k}^2}{E_N},g_1\right]. \tag{34}$$

Since $g=g_1$ on the left, this scaling law holds for all $\vec{k}^2$ and E.[12] Our task is to calculate the scaling function $\phi_{1,1}$. Since $g_1^2=O(\epsilon)$ we can determine the left side as a power series in ϵ by using perturbation theory. On the right we expand

$$\phi_{1,1}(\rho,\epsilon)=\sum_{n=0}^{\infty}\epsilon^n\phi_{1,1}^{(n)}(\rho),\qquad \rho=\left(\frac{-E}{E_N}\right)^{-Z(g_1)}\frac{\alpha'\vec{k}^2}{E_N}. \tag{35}$$

We have expressed the g_1 dependence of $\phi_{1,1}$ as an explicit dependence on ϵ in Eq. (35). Comparing powers of ϵ, we find the first two terms in the expansion of ϕ_{11} (see Ref. 7):

$$i\phi_{1,1}^{(0)}=-1-\rho,\qquad i\phi_{1,1}^{(1)}=-\tfrac{1}{12}(1+\tfrac{1}{2}\rho)[\ln(1+\tfrac{1}{2}\rho)-1]. \tag{36}$$

So far no problem is visible, but now let us rewrite Eq. (34) as

$$\Gamma_R^{(1,1)}(E,\vec{k},g_1,\alpha',E_N) = E_N\left(\frac{\alpha'\vec{k}^2}{E_N}\right)^{[1-\gamma(g_1)]/Z(g_1)}\bar{\phi}_{1,1}\left[\left(\frac{-E}{E_N}\right)^{-Z(g_1)}\frac{\alpha'\vec{k}^2}{E_N},g_1\right]. \tag{37}$$

We can expand $\bar{\phi}_{1,1}$ in a power series in ϵ like Eq. (35), with the result

$$\bar{\phi}_{1,1}(\rho,\epsilon)=\sum_{n=0}^{\infty}\epsilon^n\bar{\phi}_{1,1}^{(n)}(\rho),\qquad i\bar{\phi}_{1,1}^{(0)}=-1-\frac{1}{\rho},\qquad i\bar{\phi}_{1,1}^{(1)}=-\frac{1}{24}\left(1+\frac{2}{\rho}\right)\left[\ln\left(\frac{1}{2}+\frac{1}{\rho}\right)-1\right]-\frac{\ln\rho}{24\rho}. \tag{38}$$

Now suppose we set $E=0$ in Eq. (37). Then $\rho\to\infty$ and

$$i\Gamma_R^{(1,1)}(0,\vec{k},g_1,\alpha',E_N) = -E_N\left(1-\frac{\epsilon}{24}\right)\left(\frac{\alpha'\vec{k}^2}{E_N}\right)^{1+\epsilon/24}. \tag{39}$$

Comparing this with Eq. (34), we find that $\phi_{1,1}$ must have the asymptotic behavior

$$i\phi_{1,1}(\rho,\epsilon)\underset{\rho\to\infty}{\sim}-\left(1-\frac{\epsilon}{24}\right)(\rho)^{1+\epsilon/24}. \tag{40}$$

When this is expanded as a power series in ϵ, the first two terms resemble Eq. (36), but the expansion in powers of ϵ obviously should not be truncated. As things now stand, Eq. (35) is useful for $|\rho|\ll e^{1/\epsilon}$, while Eq. (38) is useful for $|\rho|\gg e^{-1/\epsilon}$. What is needed is an expression which agrees with Eqs. (36) and (38) in these limits and interpolates between them. We turn to that task.

Our plan is to improve upon Sec. II in two ways. In Eqs. (13a) and (13b) we normalize at a general point so we can obtain the implications of the renormalization group for a general change of normalization point. We also use the renormalization constants as the objects we study. Knowing Z_2 and Z_3, we determine the propagator through Eqs. (14). Since $Z(g=0)=1$, we avoid the undetermined boundary value on the right side of Eq. (24). The boundary value is equivalent to the scaling function in Eq. (34), so we learn what we want.[13] The improved scaling function is an infinite power series in ϵ, and it provides the interpolation between the small- and large-ρ regions.

Our new normalization conditions are

$$\left.\frac{\partial i\Gamma_R^{(1,1)}}{\partial E}\right|_{E=-E_N;\vec{k}^2=k_N^2}=1, \tag{41a}$$

$$\left.\frac{\partial i\Gamma_R^{(1,1)}}{\partial \vec{k}^2}\right|_{E=-E_N;\vec{k}^2=k_N^2}=-\alpha', \tag{41b}$$

$$\Gamma_R^{(2,1)}|_{E_1=2E_2=2E_3=-E_N;\vec{k}_i=0}=\gamma/(2\pi)^{(D+1)/2}. \tag{41c}$$

The renormalization constants are given by

$$Z_3^{-1}=\left.\frac{\partial i\Gamma^{(1,1)}}{\partial E}\right|_{E=-E_N;\vec{k}^2=k_N^2}, \tag{42a}$$

$$Z_2^{-1}=-(\alpha_0')^{-1}Z_3\left.\frac{\partial i\Gamma^{(1,1)}}{\partial k^2}\right|_{E=-E_N;\vec{k}^2=k_N^2}, \tag{42b}$$

and Z_1 still determined by Eq. (14c). Renormalized and unrenormalized parameters are still related as in Eq. (10). We introduce the bare dimensionless coupling g_0:

$$g_0=\frac{\gamma_0}{(\alpha_0')^{D/4}}E_N^{D/4-1}=Z^{-1}g,\qquad Z=Z_3^{3/2}Z_2^{D/4}Z_1^{-1}. \tag{43}$$

We also define renormalization-group functions

$$\gamma_E = \frac{\partial \ln Z_3}{\partial \ln E_N}\bigg|_B, \quad \gamma_k = \frac{\partial \ln Z_3}{\partial \ln k_N^2}\bigg|_B,$$

$$\tau_E = -\frac{\partial \ln Z_2}{\partial \ln E_N}\bigg|_B, \quad \tau_k = -\frac{\partial \ln Z_2}{\partial \ln k_N^2}\bigg|_B,$$

$$\beta_E = \frac{\partial g}{\partial \ln E_N}\bigg|_B = -\frac{\epsilon g}{4} + g\frac{\partial \ln Z}{\partial \ln E_N}\bigg|_B, \tag{44}$$

$$\beta_k = \frac{\partial g}{\partial \ln k_N^2}\bigg|_B = g\frac{\partial \ln Z}{\partial \ln k_N^2}\bigg|_B,$$

$$B = \{r_0, \alpha_0'\}.$$

Note that the renormalization constants can depend only on dimensionless parameters; we choose these as the *renormalized* parameters $x = \alpha' k_N^2/E_N$ and g. By the chain rule we have for Z_3

$$\gamma_E = \frac{\beta_E}{g}\frac{\partial \ln Z_3}{\partial \ln g} + (\tau_E - 1)\frac{\partial \ln Z_3}{\partial \ln x},$$
$$\gamma_k = \frac{\beta_k}{g}\frac{\partial \ln Z_3}{\partial \ln g} + (\tau_k + 1)\frac{\partial \ln Z_3}{\partial \ln x}. \tag{45}$$

These equations can be solved for the partial derivatives

$$\frac{\partial \ln Z_3}{\partial \ln g} = \frac{g\bar{\gamma}}{\bar{\beta}}, \tag{46a}$$

$$\frac{\partial \ln Z_3}{\partial \ln x} = \frac{\gamma_k\beta_E - \gamma_E\beta_k}{\bar{\beta}}, \tag{46b}$$

where

$$\bar{\beta} = \beta_E(1+\tau_k) + \beta_k(1-\tau_E),$$
$$\bar{\gamma} = \gamma_E(1+\tau_k) + \gamma_k(1-\tau_E) \tag{47}$$

are effective β and γ functions for the generalized normalization we use. We can now integrate Eq. (46), using the boundary condition $Z_3(g=0)=1$:

$$Z_3(g, x) = \exp\int_0^g \frac{dg'\bar{\gamma}(g', x)}{\bar{\beta}(g', x)}. \tag{48}$$

Similar calculations produce the rest of the renormalization constants

$$Z_2(g, x) = \exp\left[-\int_0^g \frac{dg'\bar{\tau}(g', x)}{\bar{\beta}(g', x)}\right], \tag{49}$$

$$Z(g, x) = \exp\left[\int_0^g \frac{dg'}{\bar{\beta}(g', x)}\left(\frac{\bar{\beta}(g', x)}{g'} + \frac{\epsilon}{4}[1+\tau_k(g', x)]\right)\right], \tag{50}$$

where

$$\bar{\tau} = \tau_E + \tau_k. \tag{51}$$

It is good to pause here and reflect on these equations. Suppose we begin a calculation with perturbation theory, which gives the Z's as power series in g_0. From these series we obtain the renormalization-group functions of Eq. (44) and then recompute the Z's in Eqs. (48)–(50). No approximations have been made, so for the exact Z's the original series will be equivalent to Eqs. (48)–(50). The only difference will be that Eqs. (48)–(50) give the Z's in terms of g rather than g_0. However, Eqs. (48)–(50) are *reformulations* which will lead to *different* expressions from the renormalization constants when approximations are made. The approximation we shall make is the usual one of truncating the perturbation theory expressions for the renormalization-group functions. In this case, Eqs. (48)–(50) are much more useful than the original (now finite) power series. The new Z's are infinite power series which are singular at the value of g for which $\bar{\beta}$ vanishes. This singularity gives us the infrared behavior we want. The progression from the finite power series to Eqs. (48)–(50) therefore goes from a less powerful to a more powerful use of the information available in perturbation theory.

We continue by rewriting the relation between renormalized and bare parameters

$$g_0 = gZ^{-1}(g, x), \tag{52a}$$

$$x_0 \equiv \frac{\alpha_0' k_N^2}{E_N} = xZ_2(g, x). \tag{52b}$$

This pair of equations has an inverse, which we write formally

$$g = \xi(g_0, x_0),$$
$$x = \eta(g_0, x_0). \tag{53}$$

Using ξ and η, we express Eqs. (42) in terms of bare parameters g_0 and x_0,

$$\frac{\partial i\Gamma^{(1,1)}}{\partial E}\bigg|_{E=-E_N;\vec{k}^2=k_N^2} = Z_3^{-1}(\xi(g_0, x_0), \eta(g_0, x_0)),$$
$$\frac{\partial i\Gamma^{(1,1)}}{\partial \vec{k}^2}\bigg|_{E=-E_N;\vec{k}^2=k_N^2} = -\alpha_0' Z_2^{-1}(\xi, \eta)Z_3^{-1}(\xi, \eta). \tag{54}$$

We examine the infrared behavior of these derivatives by letting $E_N \to 0$, with r_0 and α_0' fixed, and x_0 varying in a manner to be specified later. In the infrared limit $g_0 \to \infty$, and we need the behaviors of ξ and η as their first argument tends to infinity. We begin with Eq. (52a). As $g_0 \to \infty$, we see that either g tends to infinity, or Z vanishes. We will study the possibility that Z vanishes and later will see that this is the relevant case. Equation (50) tells us that Z vanishes when g approaches a zero of $\bar{\beta}(g, x)$. We make this quantitative by assuming that $\bar{\beta}(g, x)$ has a linear zero at $g = g_1(x)$,

$$\bar{\beta}(g, x) = \bar{\beta}'(x)[g - g_1(x)] + \text{higher terms}. \tag{55}$$

Then for g near g_1,

$$\ln Z_i = c_i(x) \ln[g_1(x) - g] + \ln \bar{Z}_i(x) + \sum_{n=1}^{\infty} a_{n,i}(x)[g - g_1(x)]^n, \tag{56}$$

where $Z_i = Z$, Z_2, or Z_3, and

$$c(x) = \frac{\epsilon}{4\bar{\beta}'}(1 + \tau_k)_1, \quad c_2(x) = -\frac{1}{\bar{\beta}'}(\bar{\tau})_1, \quad c_3(x) = \frac{1}{\bar{\beta}'}(\bar{\gamma})_1. \tag{57}$$

The suffix 1 means that $g_1(x)$ is substituted for g wherever g appears. For g near g_1,

$$Z(g, x) \sim \bar{Z}(x)[g_1(x) - g]^c. \tag{58}$$

As long as c is positive, we can invert Eq. (52a) to find

$$\xi(g_0, x_0) \underset{g_0 \to \infty}{\sim} g_1(\eta) - \left[\frac{g_1(\eta)}{g_0 \bar{Z}(\eta)}\right]^{1/c}. \tag{59}$$

Equation (59) is not yet a total inversion because η appears on the right side. We must also consider Eq. (52b). For g near g_1,

$$Z_2(g, x) \sim \bar{Z}_2(x)[g_1(x) - g]^{c_2}. \tag{60}$$

Substituting $x \to \eta$, $g \to \xi$ in Eq. (52b), we find η is determined from

$$x_0 = \eta \bar{Z}_2(\eta)\left[\frac{g_1(\eta)}{g_0 \bar{Z}(\eta)}\right]^{c_2/c}. \tag{61}$$

We rewrite Eqs. (59) and (61) in a form which specifies ξ and η as $E_N \to 0$:

$$\frac{\alpha_0' k_N^2}{E_N^{1+\epsilon c_2/4c}} = \eta \bar{Z}_2(\eta)\left[\frac{(\alpha_0')^{D/4} g_1(\eta)}{r_0 \bar{Z}(\eta)}\right]^{c_2/c}, \tag{62a}$$

$$\xi = g_1(\eta) - E_N^{\epsilon/4c}\left[\frac{(\alpha_0')^{D/4} g_1(\eta)}{r_0 \bar{Z}(\eta)}\right]^{1/c}. \tag{62b}$$

We now have the infrared behaviors of the derivatives of the inverse unrenormalized propagators, Eqs. (54):

$$\left.\frac{\partial i\Gamma^{(1,1)}}{\partial E}\right|_{E=-E_N;\, \vec{k}^2 = k_N^2} = (E_N)^{-\epsilon c_3/4c} \bar{Z}_3^{-1}(\eta) \times \left[\frac{(\alpha_0')^{D/4} g_1(\eta)}{r_0 \bar{Z}(\eta)}\right]^{-c_3/c},$$

$$\left.\frac{\partial i\Gamma^{(1,1)}}{\partial \vec{k}^2}\right|_{E=-E_N;\, \vec{k}^2 = k_N^2} = -\alpha_0'(E_N)^{-\epsilon(c_2+c_3)/4c} \bar{Z}_2^{-1}(\eta)\bar{Z}_3(\eta) \times \left[\frac{(\alpha_0')^{D/4} g_1(\eta)}{r_0 \bar{Z}(\eta)}\right]^{-(c_2+c_3)/c}, \tag{63}$$

with η given implicitly by Eq. (62a) in terms of the scaling variable $\alpha_0' k_N^2/(E_N)^{1+\epsilon c_2/4c}$. As $E_N \to 0$, this variable must vary in such a way that $\beta(g, \eta)$ continues to have a zero at $g_1(\eta)$. A sufficient condition is that the scaling variable, and hence η, remains fixed as $E_N \to 0$.

The inverse unrenormalized propagator is determined by integrating Eqs. (54) from $E' = 0$ to $E' = E$ at fixed η:

$$\Gamma^{(1,1)}(E, \vec{k}^2) = \int_0^E dE' \left(\left.\frac{\partial \Gamma^{(1,1)}}{\partial E'}\right|_{\vec{k}^2} + \left.\frac{\partial \Gamma^{(1,1)}}{\partial \vec{k}^2}\right|_E \left.\frac{\partial \vec{k}^2}{\partial E}\right|_\eta\right). \tag{64}$$

The infrared asymptotic form is

$$\Gamma^{(1,1)}(E, \vec{k}^2) = \frac{2}{1 - \epsilon c_3/4c}(-E)^{1-\epsilon c_3/4c} \bar{Z}_3^{-1}(\eta) \times \left[1 + \eta\left(1 + \frac{\epsilon c_2}{4c}\right)\right]\left[\frac{(\alpha_0')^{D/4}}{r_0}\frac{g_1(\eta)}{\bar{Z}(\eta)}\right]^{-c_3/c}. \tag{65}$$

η is given implicitly by Eq. (62a), with $\vec{k}_N^2 = \vec{k}^2$, $E_N = -E$.

It is important to note that the constants c, c_2, and c_3 of Eq. (57) are independent of x (or η). This can be quickly shown for c_3 by substituting Z_3 from Eq. (56) into Eq. (46b). Since the right side has no logarithmic singularity at $g = g_1(x)$, $dc_3(x)/dx = 0$. Analogous proofs hold for c and c_2.

In a sense, Eqs. (62a) and (65) are the desired asymptotic expressions. However, we lose all information about the x dependence of the propagator when these equations are evaluated in the first-order ϵ expansion. This dependence is retained if we work out some additional equations for the derivatives of g_1, $\bar{Z}_3$, and $\bar{Z}$ with respect to x. The derivative of g_1 can be found by substituting Z_3 from Eq. (56) into Eq. (46b) and matching the residues of both sides at the pole at $g = g_1$:

$$\frac{d \ln g_1}{d \ln x} = -\left[\frac{\beta_E}{g(1 - \tau_E)}\right]_1. \tag{66}$$

$\bar{Z}$, $\bar{Z}_2$, and $\bar{Z}_3$ are determined by evaluating

$$\left(\frac{dg_1}{d \ln x}\frac{\partial}{\partial g} + \frac{\partial}{\partial \ln x}\right) \ln Z_i \Big|_{g = g_1} \tag{67}$$

by both Eq. (56) and Eq. (46) and its analogs for β and Z_2. This yields the formulas

$$\frac{d \ln \bar{Z}}{d \ln x} = c\left(\frac{\partial}{\partial g}\frac{\beta_E}{1 - \tau_E}\right)_1 - \left[\frac{\epsilon g/4 + \beta_E}{g(1 - \tau_E)}\right]_1,$$

$$\frac{d \ln \bar{Z}_2}{d \ln x} = c_2\left(\frac{\partial}{\partial g}\frac{\beta_E}{1 - \tau_E}\right)_1 + \left(\frac{\tau_E}{1 - \tau_E}\right)_1, \tag{68}$$

$$\frac{d \ln \bar{Z}_3}{d \ln x} = c_3\left(\frac{\partial}{\partial g}\frac{\beta_E}{1 - \tau_E}\right)_1 - \left(\frac{\gamma_E}{1 - \tau_E}\right)_1.$$

To lowest order in the ϵ expansion

$$\gamma_E = 2\tau_E = -\frac{g^2}{2(8\pi)^{D/2}(1+x/2)},$$
$$\gamma_k = 2\tau_k = -\frac{g^2(x/2)}{2(8\pi)^{D/2}(1+x/2)},$$
$$\beta_E = -\frac{\epsilon g}{4} + \frac{2g^3}{(8\pi)^{D/2}} - \frac{g^3}{2(8\pi)^{D/2}(1+x/2)}, \tag{69}$$
$$\beta_k = -\frac{g^3(x/2)}{2(8\pi)^{D/2}(1+x/2)}.$$

In this approximation,

$$\bar{\beta} = -\frac{\epsilon g}{4} + \frac{3g^3}{2(8\pi)^{D/2}},$$
$$\bar{\gamma} = -\frac{g^2}{2(8\pi)^{D/2}}, \quad \bar{\tau} = -\frac{g^2}{4(8\pi)^{D/2}}. \tag{70}$$

Equations (48) through (50) yield

$$Z = \left[1 - \frac{6g^2}{(8\pi)^{D/2}\epsilon}\right]^{1/2}, \quad Z_2 = \left[1 - \frac{6g^2}{(8\pi)^{D/2}\epsilon}\right]^{1/12},$$
$$Z_3 = \left[1 - \frac{6g^2}{(8\pi)^{D/2}\epsilon}\right]^{-1/6}. \tag{71}$$

From these equations we obtain

$$c = \tfrac{1}{2} + O(\epsilon), \quad c_2 = \tfrac{1}{12} + O(\epsilon), \quad c_3 = -\tfrac{1}{6} + O(\epsilon),$$
$$g_1 = (8\pi)^{D/4}\left(\frac{\epsilon}{6}\right)^{1/2} a_1(x,\epsilon),$$
$$\bar{Z} = \left[\frac{(8\pi)^{D/2}\epsilon}{24}\right]^{-1/4} a(x,\epsilon), \tag{72}$$
$$\bar{Z}_2 = \left[\frac{(8\pi)^{D/2}\epsilon}{24}\right]^{-1/24} a_2(x,\epsilon),$$
$$\bar{Z}_3 = \left[\frac{(8\pi)^{D/2}\epsilon}{24}\right]^{1/12} a_3(x,\epsilon).$$

The small value for g_1 when ϵ is small is what justifies our use of perturbation theory for the renormalization-group functions. The functions $a(x,\epsilon)$ approach 1 as $\epsilon \to 0$. They also satisfy Eqs. (66)–(68):

$$\frac{d\ln a_1}{d\ln x} = -\frac{\epsilon}{12}\frac{x/2}{1+x/2},$$
$$\frac{d\ln a}{d\ln x} = \frac{\epsilon}{24}\frac{x/2}{1+x/2}, \tag{73}$$
$$\frac{d\ln a_2}{d\ln x} = \frac{\epsilon}{16}\frac{x/2}{1+x/2},$$
$$\frac{d\ln a_3}{d\ln x} = -\frac{\epsilon}{8}\frac{x/2}{1+x/2}.$$

The solutions of these equations are

$$g_1 = (8\pi)^{D/4}\left(\frac{\epsilon}{6}\right)^{1/2} \bar{a}_1(\epsilon)(1+x/2)^{-\epsilon/12},$$
$$\bar{Z} = \left[\frac{(8\pi)^{D/2}\epsilon}{24}\right]^{-1/4} \bar{a}(\epsilon)(1+x/2)^{\epsilon/24},$$
$$\bar{Z}_2 = \left[\frac{(8\pi)^{D/2}\epsilon}{24}\right]^{-1/24} \bar{a}_2(\epsilon)(1+x/2)^{\epsilon/16}, \tag{74}$$
$$\bar{Z}_3 = \left[\frac{(8\pi)^{D/2}\epsilon}{24}\right]^{1/12} \bar{a}_3(\epsilon)(1+x/2)^{-\epsilon/8}.$$

All we know about the $\bar{a}(\epsilon)$ is the boundary value $\bar{a}(0) = 1$. These functions will be determined in the higher-order ϵ expansion. Here we set $\bar{a}(\epsilon) = 1$. In the higher-ϵ expansion, additional factors will appear on the right side of Eqs. (74), with exponents of $O(\epsilon^n)$, $n \geq 2$.

Our expression for the inverse unrenormalized propagator is

$$\Gamma^{(1,1)}(E,\vec{k}^2) = \frac{i}{1+\epsilon/12}(-E)^{1+\epsilon/12}\left[\frac{(8\pi)^{D/2}\epsilon}{24}\right]^{1/6}\left[\frac{2(\alpha_0')^{D/4}}{r_0}\right]^{1/3}$$
$$\times[1+\eta(1+\epsilon/24)](1+\eta/2)^{\epsilon/12}, \tag{75}$$
$$\frac{\alpha_0'\vec{k}^2}{(-E)^{1+\epsilon/24}} = \left[\frac{(8\pi)^{D/2}\epsilon}{24}\right]^{1/12}\left[\frac{2(\alpha_0')^{D/4}}{r_0}\right]^{1/6}\eta(1+\eta/2)^{\epsilon/24}.$$

A number of observations can be made about this result. If we assume that the scaling variable is very small (large), and expand in a power series in ϵ, we recover Eq. (36) [Eq. (38)], aside from a renormalization. Therefore, our result "exponentiates" those power series and holds uniformly for both small and large values of the scaling variable. It is easy to show that there are no fixed cuts in the energy or momentum plane, despite the fractional powers of energy in Eq. (75). The moving cut is the two-Pomeron cut. It can be shown that the pole and cut trajectories are related by the familiar equation

$$\alpha_c(t) = 2\alpha_p(t/4) - 1. \tag{76}$$

At higher orders in the ϵ expansion multi-Pomeron cuts appear. Finally by using the explicit expression for g_1 in Eq. (74), one can show that Eq. (75) holds whenever $\vec{k}^2$, E, and ϵ are small, even when the scaling variable tends to infinity. The result follows from the fact that $g_1 = O(\epsilon^{1/2})$ on the physical sheet of the angular momentum plane when $\vec{k}^2$ and E are small.

The angular distribution of the diffraction peak in $2 \to 2$ processes can now be worked out because the dominant contribution involves only the full Pomeron propagator, according to Eq. (33),

$$\frac{d\sigma}{dt} = \frac{[\beta_1(t)\beta_2(t)]^2}{16\pi}\left(\ln\frac{s}{m_0^2}\right)^{\epsilon/6}\frac{(1+\epsilon/12)^2}{K^4[\Gamma(1+\epsilon/12)]^2}$$
$$\times F_1^2\left\{-\frac{\alpha_0' t[\ln(s/m_0^2)]^{1+\epsilon/24}}{K}\right\}, \tag{77}$$

where

$$F_1(x) = x^{-(\epsilon/12)/(1+\epsilon/24)}\Gamma\left(1+\frac{\epsilon}{12}\right) \times \int_{-i\infty}^{i\infty} \frac{dw e^{-wx^{1/(1+\epsilon/24)}}[1+\bar{\eta}/2]^{-\epsilon/12}}{(-w)^{1+\epsilon/12}[1+\bar{\eta}(1+\epsilon/24)](2i\pi)}, \tag{78}$$

$$\bar{\eta}(1+\bar{\eta}/2)^{\epsilon/24} = (-w)^{-1-\epsilon/24}, \tag{79}$$

$$K = \left[\frac{(8\pi)^{D/2}\epsilon(\alpha_0')^{D/2}}{6r_0^2}\right]^{1/12}. \tag{80}$$

In Eq. (77) we have included only the imaginary part of the amplitude. The real part of the amplitude is subordinate to the second term in Eq. (33) at high energy, so it would be inconsistent to retain the real part and ignore subdominant imaginary contributions. $F_1(x)$ is normalized so $F_1(0) = 1$. It can be put in a form suitable for computation by transforming from w to $v = 1 + 1/2\bar{\eta}$ as the variable of integration. This substitution finally eliminates the implicit function of Eq. (79). The contour integral over v can be shrunk down to a line integral:

$$F_1(x) = \frac{x^{-\epsilon/12.(1+\epsilon/24)}\Gamma(1+\epsilon/12)}{2^{2/(1+\epsilon/24)}(1+\epsilon/24)^2}\cos\phi(v_0,x)\frac{\exp\{-[x/2v_0^{\epsilon/24}(1-v_0)]^{1/(1+\epsilon/24)}\cos[(\pi\epsilon/24)/(1+\epsilon/24)]\}}{v_0^{(1+\epsilon/8)/(1+\epsilon/24)}(1-v_0)^{(1-\epsilon/24)/(1+\epsilon/24)}}$$
$$- \frac{x^{-(\epsilon/12)/(1+\epsilon/24)}\Gamma(1+\epsilon/12)}{2^{(1-\epsilon/24)/(1+\epsilon/24)}(1+\epsilon/24)}\frac{P}{\pi}\int_0^1 \frac{dv\sin\phi(v,x)|(1+\epsilon/24)v-\epsilon/24|}{v^{(1+\epsilon/8)/(1+\epsilon/24)}(1-v)^{(1-\epsilon/24)/(1+\epsilon/24)}}$$
$$\times\frac{\exp\{-[x/2v^{\epsilon/24}(1-v)]^{1/(1+\epsilon/24)}\cos[(\pi\epsilon/24)/(1+\epsilon/24)]\}}{|(1+\epsilon/24)v-\frac{1}{2}-\epsilon/24|}, \tag{81}$$

$$\phi(v,x) = \frac{\pi\epsilon/12}{1+\epsilon/24} - \left[\frac{x}{2v^{\epsilon/24}(1-v)}\right]^{1/(1+\epsilon/24)}\sin\left(\frac{\pi\epsilon/24}{1+\epsilon/24}\right),$$

$$v_0 = \frac{1}{2}\frac{1+\epsilon/12}{1+\epsilon/24}.$$

We exhibit $F_1^2(x)$ in Fig. 5. At sufficiently high energy, where shrinkage is great, $F_1^2(x)$ determines the diffraction peak. It is encouraging that it has a forward peak which is six orders of magnitude above the second maximum, much as is seen in the data.

IV. THE ENERGY-NONCONSERVING TRIPLE-POMERON VERTEX

The energy-nonconserving vertex is the second function we need to assemble the leading contribution of Fig. 4. The calculation is a straightforward generalization of what has been done in Sec. III, so we will simply list some key equations along the way.

The normalization we use is that of Eq. (41), except we now set $E_N = E_1$, and $k_N^2 = \vec{k}^2$, where $-E_1$ is the energy entering the nonconserving vertex, and $\pm\vec{k}$ are the momenta flowing out. The renormalization constants are given by Eqs. (42a), (42b), (14c), and there is a new constant related to the energy-nonconserving vertex:

$$Z_0^{-1} = (2\pi)^{(D+1)/2}(r_0)^{-1} \times \tilde{\Gamma}^{(2,1)}(-E_1, -E_2, -E_3, 0, \vec{k}^2, \vec{k}^2, r_0, \alpha_0'). \tag{82}$$

$z_0 = z_1$ when $E_2 = E_3 = E_1/2$, $\vec{k}^2 = 0$. Renormalization-group functions associated with Z_0 must be defined:

$$\mu_{E_i} = \left.\frac{\partial \ln Z_0}{\partial \ln E_i}\right|_B, \quad \mu_k = \left.\frac{\partial \ln Z_0}{\partial \ln \vec{k}^2}\right|_B. \tag{83}$$

The treatment of Z, Z_2, and Z_3 is unchanged from Sec. III. Z_0 depends upon the renormalized parameters g and λ plus the two new ratios

$$\lambda_2 = E_2/E_1, \quad \lambda_3 = E_3/E_1. \tag{84}$$

The differential equations satisfied by Z_0 are

$$\frac{\partial \ln Z_0}{\partial \ln g} = \frac{g\bar{\mu}}{\bar{\beta}}, \quad \frac{\partial \ln Z_0}{\partial \ln x} = \frac{\mu_k\beta_E - (\Sigma\mu_E)\beta_k}{\bar{\beta}},$$
$$\frac{\partial \ln Z_0}{\partial \ln \lambda_i} = \mu_{E_i}, \tag{85}$$

where

$$\bar{\mu} = (\Sigma\mu_E)(1+\tau_k) + \mu_k(1-\tau_E). \tag{86}$$

Thus

$$Z_0(g,x,\lambda_i) = \exp\left(\int_0^g \frac{dg'\bar{\mu}(g',x,\lambda_i)}{\bar{\beta}(g',x)}\right). \tag{87}$$

The unrenormalized energy-nonconserving vertex is given by

$$\tilde{\Gamma}^{(2,1)}(-E_1, -E_2, -E_3, 0, \vec{k}^2, \vec{k}^2, r_0, \alpha_0') = \frac{r_0}{(2\pi)^{(D+1)/2}}Z_0^{-1}(\xi(g_0,x), \eta(g_0,x), \lambda_i). \tag{88}$$

The infrared limit is studied as in Sec. III, with

the result

$$\tilde{\Gamma}^{(2,1)}(-E_1, -E_2, -E_3, 0, \vec{k}^2, \vec{k}^2, r_0, \alpha_0') = \frac{r_0}{(2\pi)^{(D+1)/2}}(E_1)^{-\epsilon c_0/c}\bar{Z}_0^{-1}(\eta, \lambda_i) \times\left[\frac{(\alpha_0')^{D/4}}{r_0}\frac{g_1(\eta)}{\bar{Z}(\eta)}\right]^{-c_0/c}, \quad (89a)$$

$$\frac{\alpha_0'\vec{k}^2}{(E_1)^{1+\epsilon c_2/4c}} = \eta\bar{Z}_2(\eta)\left[\frac{(\alpha_0')^{D/4}}{r_0}\frac{g_1(\eta)}{\bar{Z}(\eta)}\right]^{c_2/c} \quad (89b)$$

$$C_0 = \frac{1}{\beta'}(\bar{\mu})_1. \quad (89c)$$

One can show that c_0 is independent of both x and λ_i. In the ϵ expansion we will also need the differential equations for the parameter dependence of $\bar{Z}_0$:

$$\frac{\partial \ln \bar{Z}_0}{\partial \ln x} = c_0\left(\frac{\partial}{\partial g}\frac{\beta_E}{1-\tau_E}\right)_1 - \left(\frac{\Sigma\mu_E}{1-\tau_E}\right)_1,$$
$$\frac{\partial \ln \bar{Z}_0}{\partial \ln \lambda_i} = (\mu_{E_i})_1. \quad (90)$$

When calculating in the lowest-order ϵ expansion, the only new feature is the evaluation of the "energy-conserving diagrams" of Fig. 6. The new renormalization-group functions are

$$\mu_{E_i} = -\frac{g^2}{(8\pi)^{D/2}}\int_0^1 dy\, y\left(\frac{1}{A}+\frac{1}{A'}\right),$$
$$\mu_{E_2} = -\frac{g^2}{(8\pi)^{D/2}}\lambda_2\int_0^1 dy(1-y)\frac{1}{A},$$
$$\mu_{E_3} = -\frac{g^2}{(8\pi)^{D/2}}\lambda_3\int_0^1 dy(1-y)\frac{1}{A}, \quad (91)$$
$$\mu_k = -\frac{g^2}{(8\pi)^{D/2}}\frac{x}{2}\int_0^1 dy(1-y^2)\left(\frac{1}{A}+\frac{1}{A'}\right),$$

where

$$A = y + (1-y)\lambda_2 + (1-y^2)\frac{x}{2},$$
$$A' = y + (1-y)\lambda_3 + (1-y^2)\frac{x}{2}. \quad (92)$$

Thus, to this order,

$$\bar{\mu} = -\frac{2g^2}{(8\pi)^{D/2}}, \quad Z_0 = \left[1 - \frac{6g^2}{(8\pi)^{D/2}\epsilon}\right]^{-2/3},$$
$$c_0 = -\tfrac{2}{3} + O(\epsilon), \quad Z_0 = \left[\frac{(8\pi)^{D/2}\epsilon}{24}\right]^{1/3} a_0(x, \lambda_i). \quad (93)$$

Equations for $a_0(x, \lambda_i)$ follow from Eqs. (90):

$$\frac{\partial \ln a_0}{\partial \ln x} = -\frac{\epsilon}{6}\frac{x/2}{1+x/2} - \frac{\epsilon}{6}\frac{x}{2}\int_0^1 dy(1-y^2)\left(\frac{1}{A}+\frac{1}{A'}\right),$$
$$\frac{\partial \ln a_0}{\partial \ln \lambda_2} = -\frac{\epsilon}{6}\lambda_2\int_0^1 dy(1-y)\frac{1}{A}, \quad (94)$$
$$\frac{\partial \ln a_0}{\partial \ln \lambda_3} = -\frac{\epsilon}{6}\lambda_3\int_0^1 dy(1-y)\frac{1}{A'}.$$

The solution of these equations is

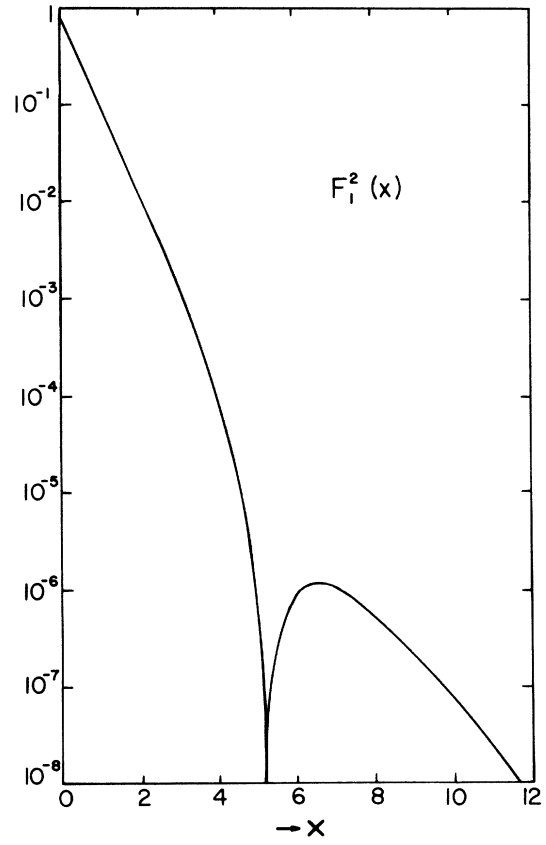

FIG. 5. The function $F_1^2(x)$ which determines the diffraction pattern in 2→2 processes at asymptotic energies. In the graph we have set $\epsilon = 2$.

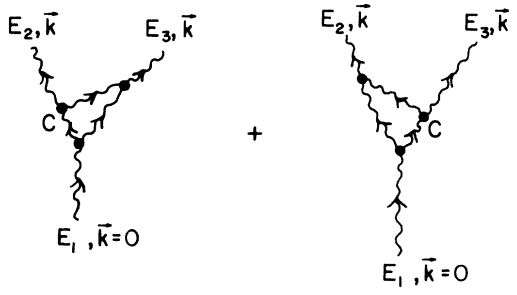

FIG. 6. Perturbation diagrams contributing μ_{E_i} and μ_k in the lowest-order ϵ expansion. The vertex C is energy nonconserving.

$$a_0 = \bar{a}_0(\epsilon)(1+x/2)^{-\epsilon/6} \times \exp\left[-\frac{\epsilon}{6}\int_0^1 dy(\ln A + \ln A')\right]. \quad (95)$$

Again we choose $\bar{a}_0(\epsilon)=1$. Our final infrared asymptotic form is

$$\tilde{\Gamma}^{(2,1)}(E_1,E_2,E_3,0,\vec{k}^2,\vec{k}^2,r_0,\alpha_0') = \frac{r_0 K^8}{(2\pi)^{(D+1)/2}}(-E_1)^{\epsilon/3}\exp\left[\frac{\epsilon}{6}\int_0^1 dy(\ln A+\ln A')\right],$$
$$\frac{\alpha'\vec{k}^2}{(-E_1)^{1+\epsilon/24}} = K\eta\left(1+\frac{\eta}{2}\right)^{\epsilon/24}. \quad (96)$$

In this equation, x is replaced by η in A and A'.

V. THE INCLUSIVE CROSS SECTION IN THE TRIPLE-REGGE REGION

The leading contribution based on our results is

$$\frac{d\sigma}{dt\,d\ln M^2} = \frac{r_0 K^2}{16\pi}\left(1+\frac{\epsilon}{12}\right)^3 \beta_1(0)\beta_2^2(t)\int_{c-i\infty}^{c+i\infty}\frac{dE_1dE_2dE_3(-E_1)^{\epsilon/3}}{(2\pi i)^3[(-E_1)(-E_2)(-E_3)]^{1+\epsilon/2}} \times \frac{\exp[-E_1\ln(M^2/m_0^2)-(E_2+E_3)\ln(s/M^2)+(\epsilon/6)\int_0^1 dy(\ln A+\ln A')]}{f(\eta_2)f(\eta_3)}, \quad (97)$$

where

$$f(\eta) = [1+\eta(1+\epsilon/24)][1+\eta/2]^{\epsilon/12},$$
$$\frac{\alpha_0'\vec{k}^2}{(-E_i)^{1+\epsilon/24}} = K\eta_i(1+\eta_i/2)^{\epsilon/24}, \quad (98)$$

and in A and A' we set $x=\eta_1$. The triple Sommerfeld-Watson integral cannot be evaluated explicitly for general t, s/M^2, and M^2/m_0^2 because the integral over A and A' links E_1, E_2, and E_3 in a complicated way. However, the key limits can be studied. Let us recall the kinematic fact that if rapidity y_0 is required for a Pomeron to appear, then the triple-Regge region is characterized by

$$\frac{y_0}{\ln(s/m_0^2)} \leq \frac{\ln(M^2/m_0^2)}{\ln(s/M^2)} \leq \frac{\ln(s/m_0^2)}{y_0}. \quad (99)$$

The ratio $\ln(M^2/m_0^2)/\ln(s/M^2)$ can be either small or large. In both these limits Eq. (97) can be evaluated.

We begin by studying the region $\ln(M^2/m_0^2) \gg \ln(s/M^2)$, which is the dangerous kinematic limit for s-channel unitarity. When the contour integral in Eq. (97) is converted to a multiple line integral, the E_1 integration is dominated by values of E_1 in the range $|E_1| \lesssim 1/\ln(M^2/m_0^2)$. The integrals over E_2 and E_3 are dominated by values $|E_2|, |E_3| \sim \max[1/\ln(s/M^2), (-\alpha_0' t/K)(1/1+\epsilon/24)]$. The first term holds near $t=0$ and stems from the exponential factor $e^{-(E_2+E_3)\ln(s/M^2)}$; the second term holds when $|t|$ is larger and the Pomeron poles and cuts have moved away from $E=0$. For any t, $|E_1|$ is negligible compared with $|E_2|$, $|E_3|$, or $|E_1\eta_1|$ in the integration over A and A'. The reason $|E_1\eta_1|$ is not negligible is that it has a finite limit as E_1 vanishes:

$$\lim_{E_1\to 0} E_1\eta_1 = -2\left(\frac{-\alpha_0' t}{2K}\right)^{1/1+\epsilon/24} \simeq E_2\eta_2 \simeq E_3\eta_3. \quad (100)$$

The last two approximate equalities are exact at $\epsilon=0$. However, since the integral over A and A' already has a coefficient of order ϵ, we are free to make the replacement $E_1\eta_1 \to E_2\eta_2$ in A and $E_1\eta_1 \to E_3\eta_3$ in A'. The three energy integrals are now uncoupled:

$$\frac{d\sigma}{dt\,d\ln M^2} = \frac{K^2 r_0(1+\epsilon/12)^3 e^{-\epsilon/3}\beta_1(0)\beta_2^2(t)}{16\pi\Gamma(1+\epsilon/12)\Gamma^2(1-\epsilon/12)}\frac{(\ln M^2/m_0^2)^{\epsilon/12}}{(\ln s/M^2)^{\epsilon/6}} \times F_2^2\left[-\frac{\alpha_0' t}{K}\left(\ln\frac{s}{M^2}\right)^{1+\epsilon/24}\right] \quad \left(\ln\frac{M^2}{m_0^2} \gg \ln\frac{s}{M^2}\right), \quad (101)$$

where

$$F_2(x) = e^{-\epsilon/6}\Gamma(1-\epsilon/12)x^{(\epsilon/12)/(1+\epsilon/24)}\int_{c-i\infty}^{c+i\infty}\frac{dW\exp[-Wx^{1/(1+\epsilon/24)}](1+\bar{\eta})^{\epsilon(1+\bar{\eta})/3\bar{\eta}}}{(2i\pi)(-W)^{1-\epsilon/12}f(\bar{\eta})} \times (1+\bar{\eta}/2)^{-\epsilon(1+\bar{\eta}/2)/3\bar{\eta}},\ (-W)^{-1-\epsilon/24} = \bar{\eta}(1+\bar{\eta}/2)^{\epsilon/24}. \quad (102)$$

$F_2(x)$ is normalized so that $F_2(0)=1$, and it is an entire function of x. We treat F_2 by the transformation used for F_1. The resulting integral is

$$F_2(x)=\left(\frac{x}{2}\right)^{(\epsilon/12)/(1+\epsilon/24)}\frac{e^{-\epsilon/6}\Gamma(1-\epsilon/12)}{1+\epsilon/24}$$
$$\times\left(\frac{\cos\phi_>(v_0,x)}{4(1+\epsilon/24)}(1-v_0)^q(v_0)^{p(v_0)}(Zv_0-1)^{r(v_0)}\exp\left\{-\left[\frac{x}{2v_0^{\epsilon/24}(1-v_0)}\right]^{1/1+\epsilon/24}\cos\left(\frac{\pi\epsilon/24}{1+\epsilon/24}\right)\right\}\right.$$
$$+\left[\frac{1}{\pi}\int_0^{1/2}dv\sin\phi_<(v,x)(1-2v)^{r(v)}+\frac{P}{\pi}\int_{1/2}^{1}dv\sin\phi_>(v,x)(2v-1)^{r(v)}\right]$$
$$\left.\times\left\{(1-v)^q(v)^{p(v)}\frac{v(1+\epsilon/24)-\epsilon/24}{[1+\epsilon/12-2v(1+\epsilon/24)]}\right\}\times\exp\left\{-\left[\frac{x}{2v^{\epsilon/24}(1-v)}\right]^{1/(1+\epsilon/24)}\cos\left(\frac{\pi\epsilon/24}{1+\epsilon/24}\right)\right\}\right), \tag{103}$$

where

$$v_0=\frac{1}{2}\frac{1+\epsilon/12}{1+\epsilon/24},\quad p(v)=-1-\frac{\epsilon}{6}+\frac{\epsilon/12}{1+\epsilon/24}+\frac{\epsilon}{6(1-v)},$$
$$q=-1-\frac{\epsilon/12}{1+\epsilon/24},\quad r(v)=\frac{\epsilon}{6}-\frac{\epsilon v}{6(1-v)},$$
$$\phi_<(v,x)=\frac{\pi\epsilon}{6}-\frac{\pi\epsilon/12}{1+\epsilon/24}-\frac{\pi\epsilon v}{6(1-v)}-\left[\frac{x}{2v^{\epsilon/24}(1-v)}\right]^{1/(1+\epsilon/24)}\sin\left(\frac{\pi\epsilon/24}{1+\epsilon/24}\right), \tag{104}$$
$$\phi_>(v,x)=-\frac{\pi\epsilon/12}{1+\epsilon/24}-\left[\frac{x}{2v^{\epsilon/24}(1-v)}\right]^{1/(1+\epsilon/24)}\sin\left(\frac{\pi\epsilon/24}{1+\epsilon/24}\right).$$

$F_2^2(x)$ is displayed in Fig. 7. It is qualitatively similar to F_1, but has a more prominent secondary maximum. In both these functions, the oscillations are due partly to the fact that the Pomeron is a pair of complex poles, and partly to interference between the poles and two-Pomeron cuts. In Eq. (101) the factor $(\ln M^2/m_0^2)^{\epsilon/12}$ is what one expects for the high-energy behavior of the Pomeron-particle total cross section.

It can be shown that $F_2^2(x)\simeq e^{-2x}$ for small x. This behavior is evident from Fig. 7, and it allows us to integrate over momenum transfer. In doing this we assume that s/M^2 is so large that the t dependence of $\beta_2^2(t)$ can be ignored (it would be easy to include the t dependence if it were exponential):

$$\int_{-\infty}^{0}\frac{d\sigma}{dt\,d\ln M^2}dt=\frac{r_0K^3(1+\epsilon/12)^3e^{-\epsilon/3}\beta_1(0)\beta_2^2(0)}{32\pi\alpha_0'\Gamma(1+\epsilon/12)\Gamma^2(1-\epsilon/12)}\frac{[\ln(M^2/m_0^2)]^{\epsilon/12}}{[\ln(s/M^2)]^{1+5\epsilon/24}}. \tag{105}$$

This can be further integrated over M^2. Let us suppose that Eq. (105) is accurate for $\ln M^2\geq p\ln s$. This gives the lower limit on M^2, and the upper limit is chosen so that at high energy the integration over t extends all the way to $x=0$. At large M^2,

$$x_{\min}=\frac{-\alpha_0't_{\max}}{K}\left(\ln\frac{s}{M^2}\right)^{1+\epsilon/24}\sim\left(\frac{M^2}{s}\right)^2\frac{\alpha_0'm_0^2}{K}\left(\ln\frac{s}{M^2}\right)^{1+\epsilon/24}. \tag{106}$$

If we choose $M^2\leq\delta s$, with δ small, we integrate arbitrarily close to $x=0$ and can use Eq. (105). This restriction also keeps s/M^2 large enough to Reggeize, and avoids multiple counting of exclusive events in the inclusive cross section. The integrated inclusive cross section is

$$\int_{p\ln(s/m_0^2)}^{\ln(s/m_0^2)-\ln(1/s)}d\ln(M^2/m_0^2)\int_{-\infty}^{0}dt\frac{d\sigma}{dt\,d\ln M^2}=\frac{3r_0K^3(1+\epsilon/12)^3e^{-\epsilon/3}\beta_1(0)\beta_2^2(0)[\ln(s/m_0^2)]^{\epsilon/12}}{20\pi\epsilon\alpha_0'\Gamma(1+\epsilon/12)\Gamma^2(1-\epsilon/12)(-\ln\delta)^{5\epsilon/24}}. \tag{107}$$

By unitarity, this cannot exceed the total cross section, and we see that it rises with the same power of $\ln(s/m_0^2)$ as the total cross section. Since the large-M^2 end of the spectrum is where a simple Pomeron pole violates unitarity, the interacting Pomeron corrects that inconsistency. The factor $1/\epsilon$ in Eq. (107) does not indicate an infinite result at $\epsilon=0$. There is another term, also proportional to $1/\epsilon$, which has been dropped in Eq. (107). This term is subordinate for $\epsilon>0$, but not at $\epsilon=0$. The factor $1/\epsilon$ is therefore associated with a Stokes's phenomenon in the asymptotic behavior at $\epsilon=0$.

The other limit we study is the triple-Regge region just above the resonances, $\ln(M^2/m_0^2) \ll \ln(s/M^2)$. We now have two subcases according to the value of t. The first case is that of large t, $(-\alpha_0' t/K)[\ln(M^2/m_0^2)]^{1+\epsilon/24} \gg 1$. In this case we can still ignore E_1 relative to E_2 and E_3 because the Pomeron poles and cuts have moved sufficiently far away from $E_{2,3}=0$. Therefore, Eq. (101) continues to apply.

The small-t region $(-\alpha_0' t/K)[\ln(M^2)]^{1+\epsilon/24} \ll 1$ leads to different approximations in the treatment of the triple-Pomeron vertex. We now drop E_2, E_3, and $E_1\eta_1$ relative to E_1 in A and A'. As a consequence, the inclusive diffraction pattern bears a close resemblance to the diffraction pattern in $2\to 2$ processes. This is expected in the resonance region, and it continues to hold into the low M^2 part of the triple-Regge region. We find for $\ln(M^2/m_0^2) \ll \ln(s/M^2)$, $(-\alpha_0' t/K)[\ln(M^2)]^{1+\epsilon/24} \ll 1$,

$$\frac{d\sigma}{dt\, d\ln M^2} = \frac{K^2 r_0 e^{-\epsilon/3}(1+\epsilon/12)^3 \beta_1(0)\beta_2^2(t)}{16\pi\Gamma(1-\epsilon/4)\Gamma^2(1+\epsilon/12)} \frac{[\ln(s/M^2)]^{\epsilon/6}}{[\ln(M^2/m_0^2)]^{\epsilon/4}} F_1^2\left[-\frac{\alpha_0' t}{K}\left(\ln\frac{s}{M^2}\right)^{1+\epsilon/24}\right]. \tag{108}$$

As before, we can integrate over t, and over $\ln M^2$ from y_0 to $p\ln s$. This contribution falls like $(\ln s)^{-\epsilon/8}$ at high energy, so the proof that s-channel unitarity is not violated is complete. Note also that when M^2 is fixed, the inclusive cross section has the same high-energy behavior as the $2\to 2$ amplitude in Eq. (76). This is expected for resonances, and it carries over into the low M^2 part of the triple-Regge region.

In Fig. 8 we show the $\ln M^2$ distribution at $t=0$. For pure Pomeron poles with $\alpha(0)=1$, this distribution is flat. In this interacting Pomeron theory it rises at the small-M^2 (resonance) and large-M^2 (Feynman $x=0$) ends of the triple-Regge region. The singularities at $M^2=0$ and $M^2=s$ lie outside the triple-Regge region.

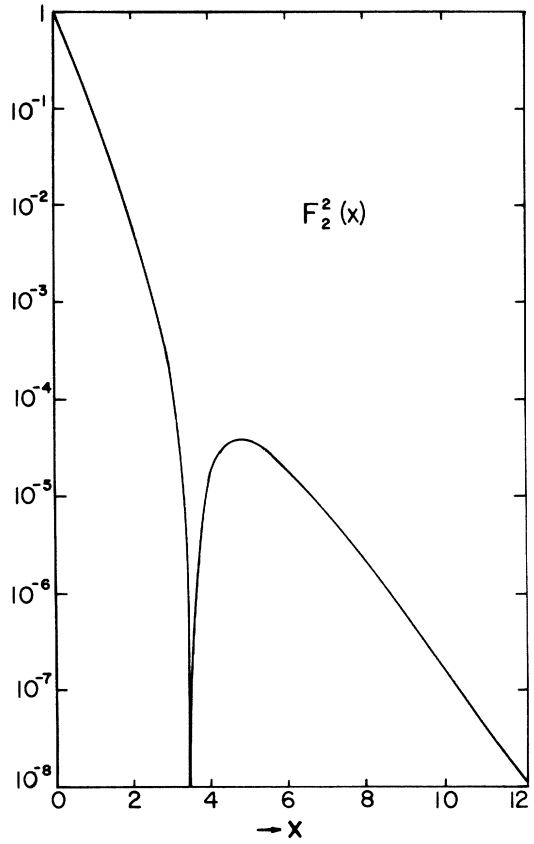

FIG. 7. The function $F_2^2(x)$ which determines the diffraction pattern in inclusive process where $\ln(M^2/m_0^2) \gg \ln(s/M^2) \gg 1$. Here $\epsilon=2$.

VI. SUMMARY AND CONCLUSIONS

We have calculated the effects of Pomeron cuts on inclusive cross sections in the triple-Regge limit using Reggeon field theory and the ϵ expansion. In the leading contribution only one Pomeron couples to each fast particle (Fig. 5), so the main task was to calculate the complete Pomeron propagator and the "energy-nonconserving" triple-Pomeron vertex. The special version of Reggeon field theory rules for the "energy-nonconserving vertex" was derived in Ref. 1.

We calculated the complete propagator and the new vertex using the renormalization group. We first used this technique to obtain scaling laws for

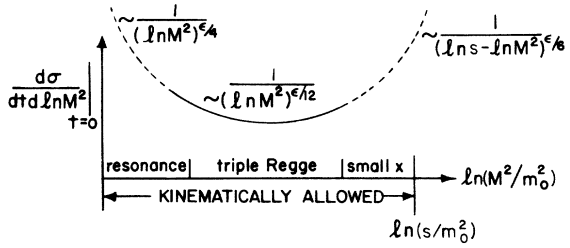

FIG. 8. The inclusive cross section in the triple-Regge region at $t=0$. The distribution for a pure Pomeron pole is a horizontal line. The middle of the triple-Regge region is an interpolation between Eqs. (101) and (108).

the inclusive amplitude. We then saw that a complete description of the M^2 and t dependencies of the amplitude would require knowledge of the scaling functions appearing in the scaling laws. In Sec. III we developed the renormalization-group machinery which permits a consistent evaluation of the scaling functions. We believe this technique may be useful for the calculation of multiparticle Green's functions in other applications of the renormalization group.

We first applied this improved technique to the calculation of the Pomeron propagator. We discovered that there is no fixed cut at $j=1$ in the angular momentum plane, even though the scaling law for the propagator hints that one is present. We were also able to calculate the leading contribution to $d\sigma/dt$ for $2\to 2$ processes. The resulting diffraction peaks show a gratifying qualitative agreement with the data.

For the inclusive cross section we were able to obtain explicit formulas when $\ln(M^2/m_0^2)$ is near either the low or high limits of the triple-Regge region. The high range is the dangerous one which leads to a violation of unitarity for a pure Pomeron pole. In our theory we find that the high range of $\ln(M^2/m_0^2)$ leads to an integrated inclusive cross section which grows at the same rate as $\sigma_{\text{tot}} \propto [\ln(s/m_0^2)]^{1/6}$. We thus confirm the finding[10] that Reggeon field theory removes the violation of unitarity. We also found that at large $\ln(M^2/m_0^2)$ and fixed t and s/M^2, the inclusive cross section grows like $[\ln(M^2/m_0^2)]^{1/6}$, that is, like the total cross section. In this region the t distribution (Fig. 7) differs substantially from $d\sigma/dt$ for exclusive processes (Fig. 5), and has a more prominent secondary maximum.

When M^2 is small (just above the resonance region), the angular distribution is the same as $d\sigma/dt$ for exclusive processes, provided t is not too large. For fixed t and M^2, the inclusive cross section grows like $[\ln(s/M^2)]^{1/6}$, that is, like the total cross section. In Fig. 8 we give an interpolation between the low- and high-M^2 limits of the triple-Regge region at $t=0$.

This is a good place to emphasize the approximations that go into our calculations, and the rather slight contact we expect our results to have with current experiments. In the first place, we evaluate only the leading behavior in the relevant partial-wave amplitude at $J_i \approx 1$, $t \approx 0$. This restriction comes about because we have calculated with a linear bare Pomeron trajectory and with only a structureless bare triple-Pomeron interaction. These terms are infrared dominant, and give the infrared behavior of almost every interacting Pomeron.[9] We do not calculate the next term in the expansion about the infrared limit, so we obtain only the leading term at high M^2/m_0^2 and s/M^2, and at small t. The crucial question, then, is how large M^2/m_0^2 and s/M^2 must be, and how small $|t|$ must be, in order for the leading term to be adequate. To answer this we must rely on reasonable estimates.

The t dependence will surely be wrong when the angular momentum of the Pomeron is changed by one unit of angular momentum because we have evaluated Pomeron signature factors at $J=1$. For this reason, a reasonable restriction is $|t| \leq 0.3$. A second reason for this restriction is that we have ignored the t dependence of the Regge couplings. Phenomenological fits generally require substantial t dependence for ordinary Regge couplings and triple-Regge vertices.

The limit on rapidity can be estimated by determining how far from $E=0$ we can trust our leading expression for the discontinuity across the cut in the energy plane in $i\Gamma^{(1,1)}$. For this estimate we set $\vec{k}^2=0$, but now we keep all the corrections to the leading infrared behavior. We do this by rewriting our expression for Z_3 in terms of the unrenormalized coupling and slope

$$Z_3 = \left[1 - \frac{6g^2}{(8\pi)^{D/2}\epsilon}\right]^{-1/6} = \left[1 + \frac{6r_0^2}{(8\pi\alpha_0')^{D/2}\epsilon E_N^{2-D/2}}\right]^{1/6}. \tag{109}$$

We can now set $D=2$ and integrate Eq. (42a):

$$i\Gamma^{(1,1)}(E,0) = -\int_0^{-E} dE' \left(1 + \frac{3r_0^2}{8\pi\alpha_0' E'}\right)^{-1/6}. \tag{110}$$

This agrees with Eq. (75) near $E=0$, but deviates strongly at the transition energy $3r_0^2/(8\pi)\alpha_0'$. Therefore, we expect our formulas to apply for rapidities

$$\ln\frac{s}{m_0^2} \sim \ln\frac{M^2}{m_0^2} \sim \ln\frac{s}{M^2} > \frac{8\pi\alpha_0'}{3r_0^2}. \tag{111}$$

When the energy is small compared to the transition energy, one should expand the integrand in Eq. (110) in ascending powers of r_0; i.e., one should use Reggeon calculus perturbation theory.

It is worth emphasizing the importance of factors such as in Eq. (111). These make a tremendous difference in the estimate for s, and it is just to get them right that we have used Eq. (110) rather than simply evaluating some typical perturbation graphs. For example, looking at the lowest-order contribution to the Pomeron self-energy would lead to $y > 16\pi\alpha_0'/r_0^2$, which is a factor of 6 larger than Eq. (111). To be sure, our estimate will change in the higher-order ϵ expansion, but we hope the factor will be less than 6. Note that the phase space factor $(8\pi)^{D/2}$ has not been expanded in powers of ϵ in this paper. It would be a serious error to have done this, for

it would have led to an extra factor of $8\pi \sim 25$ on the right side of Eq. (111).

Let us assume Reggeon perturbation theory can be used at Fermilab energies. Then for proton-proton scattering we can use the simple formulas

$$\sigma_T = \beta^2(0),$$

$$\left.\frac{d\sigma}{dt\, d\ln M^2}\right|_{t=0} = \frac{\beta^3(0)r_0}{16\pi} = \frac{(\sigma_T)^{3/2}r_0}{16\pi}. \tag{112}$$

From the data we estimate[14]

$$r_0 \approx 0.7\ \text{GeV}^{-1}. \tag{113}$$

α_0' we estimate from the slope parameter in proton-proton elastic scattering as $0.3\ \text{GeV}^{-2}$.[15] Thus we find

$$y > \frac{8\pi\alpha_0'}{3r_0^2} \sim 5. \tag{114}$$

This rapidity corresponds to $s \sim 150\ \text{GeV}^2$. It is to be emphasized that Eq. (114) is uncertain by a factor of 2 or more and is probably low. The triple-Pomeron part of the inclusive cross section, and therefore r_0, is uncertain by at least $\sqrt{2}$, and there are further corrections connected with the ϵ expansion and the fact that we have ignored multi-Pomeron couplings, t dependence of couplings, and so forth. These parameters all set rapidity scales which *must* increase the bound on y if they exceed 5. It is interesting that our estimate is much smaller than the rapidity 9 estimated by Amati and Jengo.[16] In any case, one can hope to see scaling behavior in σ_T and the $2 \to 2$ diffraction peak some day, but it is unlikely that it will be seen in inclusive processes.

We have mentioned above that for inclusive processes at present energies one should evaluate perturbation graphs. This may seem to be a simplification, but the graphs are not dominated by the triple-Pomeron coupling and the single-Pomeron coupling to fast particles. The elegant universality of the high-energy limit is lost, and one must be guided by trial and error in the construction of an adequate bare Pomeron and its interactions. The task is to restrict the number of parameters at finite energy in a believable way.

The final approximation we have made is the use of the ϵ expansion. It is more purely technical than the other approximations and one might hope to avoid it.

---

*Work supported in part by the National Science Foundation under Grant No. MPS 75-06857.

†Operated by Universities Research Association, Inc. under contract with the Energy Research and Development Administration.

[1]H. D. I. Abarbanel, J. Bartels, J. B. Bronzan, and D. Sidhu, Phys. Rev. D 12, 2459 (1975).

[2]V. N. Gribov, Zh. Eksp. Teor. Fiz. 53, 654 (1967) [Sov. Phys.—JETP 26, 414 (1968)].

[3]V. N. Gribov, I. Ya. Pomeranchuk, and K. A. Ter-Martirosyan, Phys. Rev. 139, B184 (1965).

[4]A. R. White, Nucl. Phys. B50, 93 (1972); B50, 130 (1972); P. Goddard and A. R. White, Nuovo Cimento 1A, 645 (1971); A. R. White, Nucl. Phys. B39, 432 (1972); B39, 461 (1972).

[5]J. L. Cardy, R. L. Sugar, and A. R. White, Phys. Lett. 55B, 384 (1975).

[6]L. M. Saunders *et al.*, Phys. Rev. Lett. 26, 937 (1971); C. E. Jones *et al.*, Phys. Rev. D 6, 1033 (1972).

[7]H. D. I. Abarbanel and J. B. Bronzan, Phys. Rev. D 9, 2397 (1974).

[8]The second-order ϵ expansion modifies the scaling exponent $-\gamma$ by a factor of 2. ($-\gamma$ is the exponent of $\ln s$ for the rise of σ_T.) See M. Baker, Phys. Lett. 51B, 158 (1974); J. B. Bronzan and J. Dash, *ibid.* 51B, 496 (1974). Other evaluations by J. Ellis and R. Savit, Nucl. Phys. B94, 477 (1975), and J. W. Dash and S. J. Harrington, Phys. Lett. 57B, 78 (1975), confirm this level of uncertainty.

[9]The infrared behavior we calculate fails to hold only if special conditions are imposed on the Pomeron and its interactions. See D. Calucci and R. Jengo, Nucl. Phys. B84, 413 (1975).

[10]A. A. Migdal, A. M. Polyakov, and K. A. Ter-Martirosyan, Zh. Eksp. Teor. Fiz. 67, 2009 (1974) [Report No. ITEP-102 (in English)].

[11]$Z_4 = 1$. There is no renormalization of the ordinary Regge coupling.

[12]When $g \neq g_1$ on the left side of Eq. (34) a slightly modified scaling law holds, but only when E and $\tilde{k}^2$ are small. See Ref. 7, Eqs. (84) and (97).

[13]Related representations in terms of renormalization constants have been introduced in Reggeon field theory in R. L. Sugar and A. R. White, Phys. Rev. D 10, 4074 (1974).

[14]K. Abe *et al.*, Phys. Rev. Lett. 31, 1088 (1973). The total proton-proton cross section is 40 mb at Fermilab energies.

[15]V. Bartenev *et al.*, Phys. Rev. Lett. 31, 1088 (1973).

[16]D. Amati and R. Jengo, Phys. Lett. 56B, 465 (1975).